PHYSICAL REVIEW B **91**, 201110(R) (2015)

g-factor modification in a bulk InGaAs epilayer by an in-plane electric field

M. Luengo-Kovac,[1] M. Macmahon,[1] S. Huang,[2] R. S. Goldman,[2] and V. Sih[1]
[1]*Department of Physics, University of Michigan, Ann Arbor, Michigan 48109, USA*
[2]*Department of Materials Science and Engineering, University of Michigan, Ann Arbor, Michigan 48109, USA*
(Received 25 January 2015; revised manuscript received 12 May 2015; published 26 May 2015)

We report on the modification of the g factor by an in-plane electric field in an $In_{0.026}Ga_{0.974}As$ epilayer. We performed external magnetic field scans of the Faraday rotation of the InGaAs film in order to independently determine the g factor and the spin-orbit fields. The g factor increases from -0.4623 ± 0.0001 at 0 V/cm to -0.4570 ± 0.0001 at 40 V/cm applied along the $[1\bar{1}0]$ crystal axis. The change in g factor with electric field can have a large effect on the determination of the internal spin-orbit and nuclear fields from Larmor precession frequency measurements.

DOI: 10.1103/PhysRevB.91.201110 PACS number(s): 72.25.Dc, 71.70.Ej, 71.70.Fk, 72.25.Rb

The field of spintronics is based on the manipulation of spins by electric and magnetic fields. The strength of the interaction of a spin with a magnetic field is determined by the g factor. Therefore, local manipulation of the g factor allows for local control of spins. Electron spin resonance (ESR) was shown to induce spin flips in a quantum dot when the frequency of an oscillating magnetic field matched the resonance frequency of the spin in a perpendicular static magnetic field, $g\mu_B B_{\text{stat}} = hf_{\text{osc}}$ [1]. As this technique requires high magnitude, high frequency magnetic fields, alternative methods were developed that instead used an alternating electric field to produce the resonance, either by creating an oscillating spin-orbit (SO) field [2] or by electrically modulating the g tensor, called g-tensor modulation resonance (g-TMR) [3]. The use of an electric field also allows for more local manipulation than that possible with magnetic fields [4].

g-TMR requires electrical control of the g factor, which has been demonstrated in quantum wells (QWs) [5] and quantum dots (QDs) [6] but not in bulk materials. In QWs and QDs, the change in the g factor can be attributed to the shifting of the wave function into the barrier, which has a different g factor, by an electric field. In this paper, we demonstrate electrical control of the g factor in a bulk $In_{0.026}Ga_{0.974}As$ epilayer. We characterize the g-factor dependence on the in-plane electric field and drift velocity using magnetic field and spatially resolved pump-probe Faraday rotation spectroscopy. Our results for bulk InGaAs demonstrate that the electric field dependence here must be due to a different mechanism than the wave function shift. A change in the g factor with in-plane electric field was recently reported in a QW [7].

Understanding the change in the g factor as a function of the electric field is also important to correctly determine the magnitude of the internal effective magnetic fields produced by spin-orbit coupling and nuclear spin polarization. Fits for the internal fields from time-resolved Faraday/Kerr rotation data [8–10] assume that the g factor is constant and that any measured change in the spin precession frequency is due to the internal fields. In Ref. [11], the g factor is known not to change, but the precession frequency changes due to a change in the internal fields by an electric field. However, this is referred to as an effective tuning of the g factor, using the relationship $g_{\text{eff}}(E)B_{\text{ext}} = g[B_{\text{ext}} + B_{\text{int}}(E)]$. Our measurement technique enables us to distinguish changes in the g factor from changes in the spin-orbit field.

Measurements were performed on a 500 nm thick Si-doped $In_{0.026}Ga_{0.974}As$ epilayer grown by molecular beam epitaxy on a (001) GaAs substrate. Hall measurements determined that the carrier density is 6.72×10^{15} cm$^{-}3$, and the mobility is 5700 cm^2/(Vs) at room temperature.The sample was etched in a cross pattern oriented along the [110] and $[1\bar{1}0]$ crystal axes, and ohmic contacts were deposited to apply an in-plane voltage along the [110] and $[1\bar{1}0]$ directions [Fig. 1(a)].

The g factor of the spins is measured using a Faraday rotation setup. A mode-locked Ti:sapphire laser, with a 76 MHz repetition rate, tuned to 837.08 nm, is split into pump and probe beams. A mechanical delay line is used to control the temporal separation of the pump and probe. For our magnetic field-dependent measurements, the temporal separation of the pump and probe is set to 13 ns. In order to induce a spin polarization in the sample according to the optical selection rules [12], the pump is circularly polarized. The Faraday rotation of the linearly polarized probe is measured using a balanced photodiode bridge. The pump and probe are modulated by a photoelastic modulator and an optical chopper respectively for cascaded lock-in detection. The spatial separation of the pump and probe is controlled with a scanning mirror.

For photoluminescence (PL) measurements, the sample is excited with a 633 nm HeNe laser. The spectrum is analyzed using a spectrometer with a silicon CCD. Both Faraday rotation and PL measurements are performed at 30 K, unless otherwise noted.

In the absence of internal fields, both time-resolved and magnetic field-dependent Faraday rotation measurements can be described by the equation [13]

$$\theta_F(\Delta t, B_{\text{ext}}) = \sum_n A\, e^{-(\Delta t + nt_{\text{rep}})/T_2^*} \times \cos\left[\frac{g\mu_B}{\hbar} B_{\text{ext}}(\Delta t + nt_{\text{rep}})\right], \quad (1)$$

where A is the Faraday rotation amplitude, Δt is the time delay of the pump and probe, $t_{\text{rep}} = 13.16$ ns is the laser repetition rate, T_2^* is the spin lifetime, g is the electron g factor, μ_B is the Bohr magneton, $\hbar$ is the reduced Planck's constant, B_{ext} is the magnitude of the external magnetic field, and n is the pulse number.

When an in-plane voltage is applied across the sample, the spin packets created by subsequent pump pulses will be

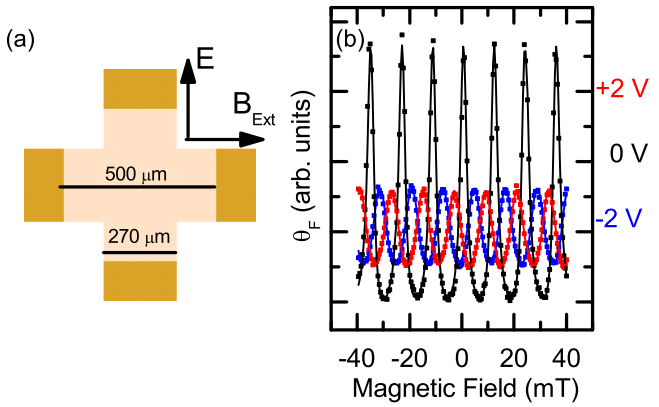

FIG. 1. (Color online) (a) Cross pattern with arms along [110] and [1$\bar{1}$0] was etched on the sample, with contacts shown in gold. The electric field was always applied perpendicular to the external magnetic field. (b) Faraday rotation data as a function of the external magnetic field for applied voltages of −2 V (blue), 0 V (black), and 2 V (red) and fits to Eq. (2).

spatially separated due to carrier drift. Equation (1) is modified to account for a spatially and time-dependent amplitude $A_n(x,\Delta t)$. Furthermore, the spins experience a momentum-dependent spin-orbit splitting that acts like an effective internal magnetic field, requiring that the external magnetic field in Eq. (1) be replaced by a vector sum of the internal and external magnetic fields [14]:

$$\theta_k(B_{\rm ext},x) = \sum_n A_n(x,\Delta t) \times \cos\left[\frac{\mu_B}{\hbar}\sqrt{g_\parallel^2(\vec{B}_{\rm ext}+\vec{B}_\parallel)^2+g_\perp^2\vec{B}_\perp^2}(\Delta t+nt_{\rm rep})\right], \quad (2)$$

where $\vec{B}_\parallel$ and $\vec{B}_\perp$ are the components of the internal field parallel and perpendicular to the external field, respectively. This equation is only valid if the parallel and perpendicular directions are eigenstates of the g-factor tensor (i.e., [110] and [1$\bar{1}$0]).

Varying Δt at a fixed $B_{\rm ext}$ results in oscillations that are periodic in $\frac{g\mu_B}{\hbar}\sqrt{(\vec{B}_{\rm ext}+\vec{B}_\parallel)^2+\vec{B}_\perp^2}$. If instead Δt is fixed and $B_{\rm ext}$ is varied, when $B_\perp = 0$, then the oscillations are periodic in $\frac{g\mu_B}{\hbar}\Delta t$.

The components of the spin-orbit field parallel and perpendicular to the external field shift the curve [Fig. 1(b)] and decrease the magnitude of the center peak, respectively, whereas the g factor changes the frequency of the peaks. In this way, unlike in time-resolved measurements, we can separately determine the g factor and the spin-orbit field.

Magnetic field scans were performed at different pump-probe separations, with the external magnetic field perpendicular to the applied voltage. Since the spin-orbit field is perpendicular to the momentum for both [110] and [1$\bar{1}$0], the spin-orbit field will be parallel to the external magnetic field. The amplitude as a function of this separation [Fig. 2(a)] shows the profile of the spin packet.

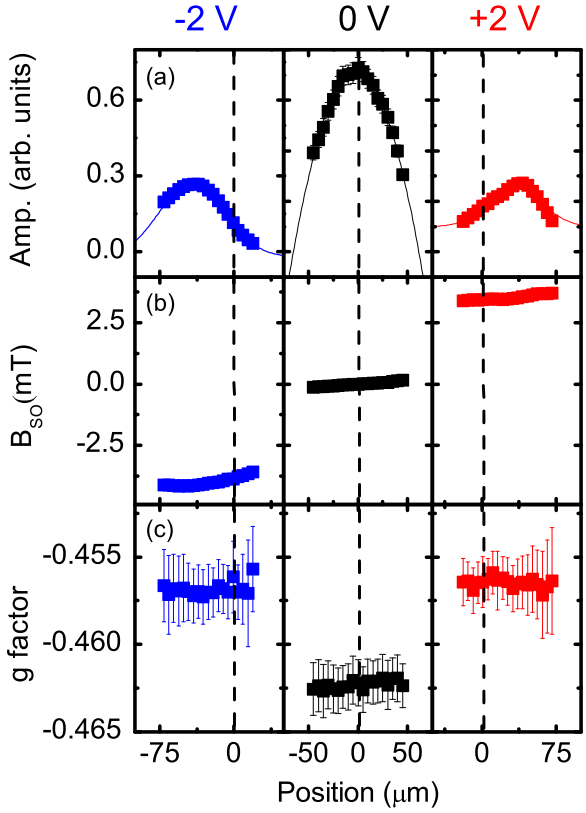

FIG. 2. (Color online) (a) Amplitude of the Faraday rotation, (b) fits of the internal field, and (c) fits of the g factor as a function of pump-probe separation for −2 V, 0 V, and +2 V along [110].

The average drift velocity (v_d) of the electrons can be calculated as a function of voltage from the center position (x_c) of the amplitude and the known temporal separation of the pump and probe pulses. From measurements of the drift velocity as a function of applied electric field, we determine the effective mobility, using the equation $\mu_{\rm eff} = v_d/E_{\rm applied}$, to be 6200 ± 200 cm^2/(V s) along the [110] direction and 5070 ± 20 cm^2/(V s) along the [1$\bar{1}$0] direction. The difference in mobilities along the two directions comes from a discrepancy between the total applied voltage and the actual voltage across the channel, as there is likely also a voltage drop across the contacts that is different for different contacts. As such, all electric field dependent measurements are presented in terms of the drift velocity, which we can measure directly.

The spin-orbit field was determined using the method described in Ref. [15] [Fig. 2(b)]. The internal fields were found to be perpendicular to the direction of the current for both [110] and [1$\bar{1}$0], as is expected for these directions. The spin-orbit field proportionality constants were found to be 1.38 ± 0.02 mT ns μm^{-1} for an electric field applied along [110] and 0.27 ± 0.01 mT ns μm^{-1} along [1$\bar{1}$0] [Fig. 3(b)].

The g factor was also extracted from the external magnetic field scan at each pump-probe spatial separation [Fig. 2(c)]. The g factor at the center of the spin packet is plotted versus the drift velocity v_d [Fig. 3(a)]. Parabolic fits are shown as a guide to the eye. However, a numerical derivative shows that this fit is less accurate for larger drift velocities. Measurements conducted along the [110] and [1$\bar{1}$0] crystal axes show similar

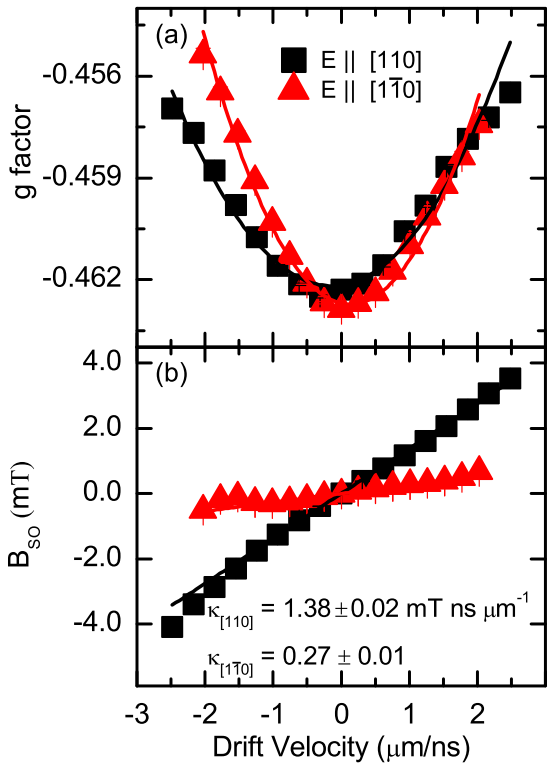

FIG. 3. (Color online) (a) g factor as a function of electric field (shown in terms of the drift velocity) for the [110] and [1$\bar{1}$0] directions. The parabolic fits to the g factor are a guide to the eye and are less accurate at higher drift velocities. (b) The internal field magnitude as a function of drift velocity. The slopes of the lines give the spin-orbit field proportionality constant.

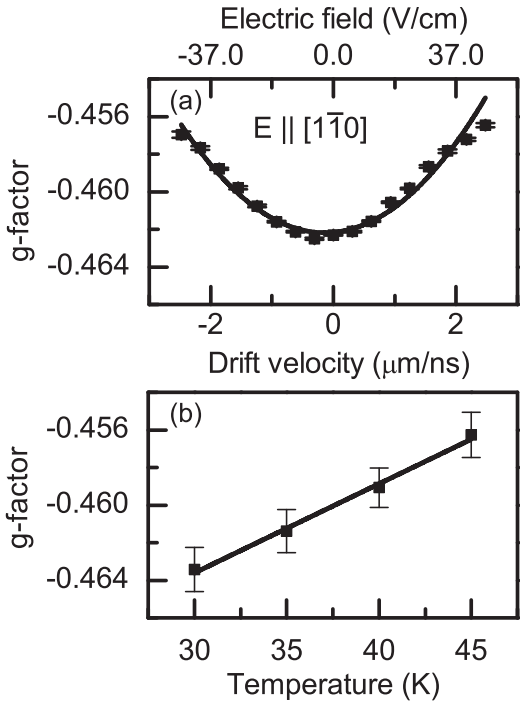

FIG. 4. (a) g factor as a function of drift velocity along [1$\bar{1}$0] at 30 K, with a parabolic fit as a guide to the eye. (b) Temperature dependence of the g factor for $v_d = 0$. The change in g factor due to an applied voltage of 2 V at 30 K corresponds to the change due to heating the sample by 15 K.

curvatures: $(1.05 \pm 0.62) \times 10^{-3}/(\frac{\mu m}{ns})^2$ for [110] and $(1.72 \pm 0.76) \times 10^{-3}/(\frac{\mu m}{ns})^2$ for [1$\bar{1}$0].

Reference [16] indicates that the energy dependence of the g factor in GaAs is given by $g^*(E) = g^* + 6.3\ \mathrm{eV}^{-1}\ E$. If we assume a parabolic dispersion relation for our values of k, then our measured dependence on the energy, taken from electric-field dependent measurements, is more than 500 times larger.

Measurements for both positive and negative v_d show that the change in g factor is symmetric about zero drift velocity [Figs. 3(a) and 4(a)], and thus only depends on the magnitude of v_d, not the direction. Temperature-dependent measurements of the g factor [Fig. 4(b)] were performed on the same channel in order to compare the effects of temperature and electric field. The change in g factor due to an applied voltage of 2 V at 30 K is equivalent to the change due to the channel heating by 15 K. From power dissipation calculations, we can estimate that the expected change in temperature of the channel due to an applied voltage of 1 V is $O(10^{-4})$ K. Therefore, the g-factor dependence on voltage and temperature are likely distinct phenomena.

To check whether the applied voltage was causing excessive channel heating, we performed temperature and voltage dependent PL measurements on a similar sample. From 30 K to 40 K, there was a clear shift in the energy of the peak due to the change in the band gap with lattice temperature. However, the PL for 0 V and 2 V had no discernible shift. Therefore, it is unlikely that the applied voltage is causing sufficient channel heating to account for the change in the g factor.

We expect the electron temperature to be significantly above the lattice temperature for our range of applied electric fields, and one possible explanation for the change in g factor is that the g factor is dependent on the electron temperature. It was reported that in n-GaAs the electron temperature increased from 4.2 K at 0 V/cm to 38 K at 20 V/cm and 75 K at 50 V/cm [17]. The electron temperature was estimated from the high energy tail of the PL. We saw no change in the PL of our sample as a function of electric field. However, we expect the PL of our sample to have greater broadening due to it being an alloy. The broadening due to alloy fluctuations could be overwhelming any changes due to the electric field.

The electron temperature can be estimated if the energy loss rate per electron is known, based on measurements done on AlGaAs/GaAs heterostructures using PL [18], Shubnikov–de Haas oscillations [19], and far-infrared spectroscopy [20]. For an applied voltage of 2 V, we found the energy loss rate per electron in our samples to be 2×10^{-12} W, which corresponds to an electron temperature of about 50 K for a lattice temperature of 4.2 K.

Another possible explanation is that the applied electric field is modifying the wave function of donor-bound electrons, thus changing the g factor [21]. Calculations for a Si dopant in GaAs show that the relative magnitude change in the g factor is comparable to what we measure here. However, the sign of the change is opposite. Furthermore, for the doping density of the sample and at the temperatures considered

here, contributions from donor-bound electrons are expected to be minimal. Therefore, we can rule out modification of donor-bound electron wave functions as the cause of the g-factor modification.

The orbital contribution of spin-orbit induced circulating currents was shown to be significant in calculations of the g factor in quantum dots [22]. Similarly, the net drift velocity of the spins in our sample could be modifying the orbital contribution to the g factor.

We have performed electric-field dependent measurements of the g factor in a bulk $In_{0.031}Ga_{0.969}As$ epilayer in a manner that distinguishes between changes in the g factor from changes in the spin-orbit field. Separate determination of these two quantities is important as their percent change with voltage is comparable. For example, for measurements along the [110] direction (Fig. 3), we found the g factor to be -0.4565 ± 0.0001 and the SO field to be 3.53 ± 0.01 mT for the largest drift velocity. If instead time-resolved measurements had been done to determine the SO field from the Larmor precession frequency with an applied magnetic field of 0.2 T assuming the zero field value of the g factor, the SO field would have been calculated to be only 0.965 ± 0.054 mT. However, more work is needed to develop a quantitative model for this phenomenon.

This work was supported by the National Science Foundation Materials Research Science and Engineering Center program No. DMR-1120923, the Office of Naval Research, the Air Force Office of Scientific Research, and the Defense Threat Reduction Agency Basic Research Grant No. HDTRA1-13-1-0013. S.H. and R.S.G. were supported in part by the Center for Solar and Thermal Energy Conversion, an Energy Frontier Research Center funded by the US Department of Energy Office of Science, Office of Basic Energy Sciences under Grant No. DE-SC0000957.

[1] F. H. L. Koppens, C. Buizert, K. J. Tielrooij, I. T. Vink, K. C. Nowack, T. Meunier, L. P. Kouwenhoven, and L. M. K. Vandersypen, Nature (London) **442**, 766 (2006).

[2] M. Schulte, J. G. S. Lok, G. Denninger, and W. Dietsche, Phys. Rev. Lett. **94**, 137601 (2005).

[3] Y. Kato, R. C. Myers, D. C. Driscoll, A. C. Gossard, J. Levy, and D. D. Awschalom, Science **299**, 1201 (2003).

[4] K. C. Nowack, F. H. L. Koppens, Yu. V. Nazarov, and L. M. K. Vandersypen, Science **318**, 1430 (2007).

[5] G. Salis, Y. Kato, K. Ensslin, D. C. Driscoll, A. C. Gossard, and D. D. Awschalom, Nature (London) **414**, 619 (2001).

[6] R. S. Deacon, Y. Kanai, S. Takahashi, A. Oiwa, K. Yoshida, K. Shibata, K. Hirakawa, Y. Tokura, and S. Tarucha, Phys. Rev. B **84**, 041302(R) (2011).

[7] Y. S. Chen, S. Fält, W. Wegscheider, and G. Salis, Phys. Rev. B **90**, 121304(R) (2014).

[8] M. Studer, M. P. Walser, S. Baer, H. Rusterholz, S. Schön, D. Schuh, W. Wegscheider, K. Ensslin, and G. Salis, Phys. Rev. B **82**, 235320 (2010).

[9] C. J. Trowbridge, B. M. Norman, Y. K. Kato, D. D. Awschalom, and V. Sih, Phys. Rev. B **90**, 085122 (2014).

[10] L. Meier, G. Salis, I. Shorubalko, E. Gini, S. Schön, and K. Ensslin, Nat. Phys. **3**, 650 (2007).

[11] Z. Wilamowski, H. Malissa, F. Schäffler, and W. Jantsch, Phys. Rev. Lett. **98**, 187203 (2007).

[12] *Optical Orientation*, edited by F. Meier and B. P. Zakharchenya (Elsevier, Amsterdam, 1984).

[13] J. M. Kikkawa and D. D. Awschalom, Phys. Rev. Lett. **80**, 4313 (1998).

[14] Y. Kato, R. C. Myers, A. C. Gossard, and D. D. Awschalom, Nature (London) **427**, 50 (2004).

[15] B. M. Norman, C. J. Trowbridge, J. Stephens, A. C. Gossard, D. D. Awschalom, and V. Sih, Phys. Rev. B **82**, 081304(R) (2010).

[16] J. Hübner, S. Döhrmann, D. Hägele, and M. Oestreich, Phys. Rev. B **79**, 193307 (2009).

[17] K. Aoki, Y. Okuyama, T. Kobayashi, and K. Yamamoto, Solid State Commun. **25**, 717 (1978).

[18] J. Shah, A. Pinczuk, H. L. Störmer, A. C. Gossard, and W. Wiegmann, Appl. Phys. Lett. **42**, 55 (1983).

[19] H. Sakaki, K. Hirakawa, J. Yoshino, S. P. Svensson, Y. Sekiguchi, T. Hotta, and S. Nichii, Surf. Sci. **142**, 306 (1984).

[20] K. Hirakawa, M. Grayson, D. C. Tsui, and Ç Kurdak, Phys. Rev. B **47**, 16651 (1993).

[21] A. De, C. E. Pryor, and M. E. Flatté, Phys. Rev. Lett. **102**, 017603 (2009).

[22] J. van Bree, A. Yu. Silov, P. M. Koenraad, and M. E. Flatté, Phys. Rev. Lett. **112**, 187201 (2014).